PCCP

COMMUNICATION

View Article Online
View Journal | View Issue

Cite this: *Phys. Chem. Chem. Phys.*, 2022, **24**, 20025

Received 29th May 2022,
Accepted 12th August 2022

DOI: 10.1039/d2cp02430f

rsc.li/pccp

Artificial synthesis of covalent triazine frameworks for local structure and property determination†

Catherine Mollart, Sarah Holcroft, Michael J. G. Peach, Adam Rowling and Abbie Trewin *

Here we show an 'artificial synthesis' method for covalent triazine framework (CTF) materials, enabling localised structural features to be incorporated that result directly from the acid-catalysed synthetic protocol that would otherwise not be captured. This advancement will enable prediction and design of new CTF materials with targeted properties.

Microporous materials, including metal–organic frameworks (MOFs),[1] covalent organic frameworks (COFs),[2] and microporous organic polymers (MOPs), have potential applications for gas adsorption, heterogeneous catalysis, and chemical separations.[3] MOPs have been shown to be very robust with good physicochemical stabilities. A number of different MOPs have been developed showing the wide synthetic diversity that is available, including hyper-crosslinked polymers (HCPs),[4] porous aromatic frameworks (PAFs),[5] conjugated microporous polymers (CMPs),[6] polymers of intrinsic microporosity (PIMs),[7] and covalent triazine-based frameworks (CTFs).[8] High surface area CTFs, approaching 3000 $m^2\ g^{-1}$ apparent BET surface area in some cases, have been reported using ionothermal synthesis with molten $ZnCl_2$ as the solvent and catalyst at high temperatures of 400–700 °C.[8,9] However, these harsh conditions and long reaction times limit monomer choice and hence practical applications. CTFs have particular potential applications in carbon dioxide capture due to its high affinity to the triazine rings of the CTF.[10]

A series of CTFs, P1–P5, were synthesised by Cooper *et al.* using trifluoromethanesulfonic acid (TFMS) as the catalyst under both room temperature and microwave-assisted conditions.[11] The structure of P1 is shown in Fig. 1 and in more detail in Fig. S1 (ESI†). These mild synthetic conditions allow for a wide range of functional group diversity to be incorporated that were previously intolerant to the harsh ionothermal conditions.

High surface area materials can be targeted through the use of monomers that have short rigid three-dimensional linkers that inhibit network interpenetration.[12] A previous structural study of P1–P5 CTFs showed that the surface area could be directly related to a combination of linker length (shorter lengths gave higher surface areas) and nodal dimensionality (high dimensionality gave higher surface areas).[13] However, the models generated in this study were based upon 'pre-formed' triazine building block units rather than real-world cyano-based monomers. This oversimplification assumes that all monomers react to fully form triazine rings, with no intermediate structures forming, and discards templating effects of unreacted monomers that can influence the resulting structure. Furthermore, characterisation of the synthesised materials shows evidence of ring formation in intermediate chemical structures that could influence system properties. It is therefore essential the potential for these intermediate structures be included in any system modelling so that their properties can be fully understood and accounted for, particularly when predicting new materials with targeted properties.

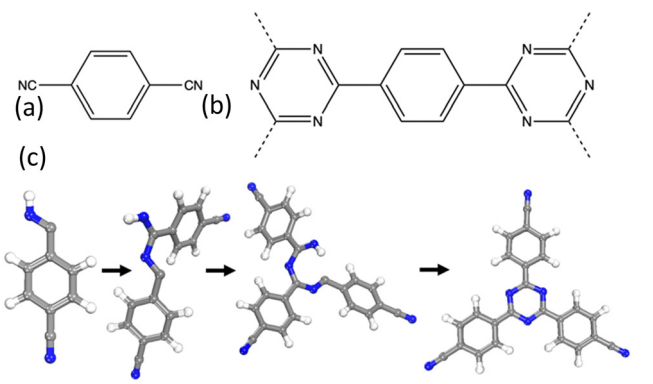

Fig. 1 (a) The monomer used for the synthesis of CTF-1/P1. (b) The repeat structure of the CTF-1/P1 polymer. (c) The test system used to model the triazine ring formation in the CTF-1/P1 polymer.

Department of Chemistry, Lancaster University, Lancaster, UK LA1 4YB, UK.
E-mail: a.trewin@lancaster.ac.uk

† Electronic supplementary information (ESI) available. See DOI: https://doi.org/10.1039/d2cp02430f

Here, we present an artificial synthetic method by which the proton-catalysed triazine ring formation mechanism is fully mimicked. This is a complex multi-step process that will allow us to explore localised structural features that otherwise would not be included in our models, and thereby gain greater understanding of the triazine materials. It will also allow us to predict the local structural and chemical features present in target CTF systems.

Computational method

Structure generation processes are challenging to model. Previous studies include utilising a kinetic Monte Carlo (KMC) approach to generate the crystalline structure of a covalent organic framework, COF-5.[14] However, the generation of the COF-5 framework structure proceeds *via* a relatively simple 1-step condensation reaction. While the resulting idealised topologies are similar, CTF-1 is generated *via* a complex multistep acid catalysed process and so a KMC approach is not appropriate.

Previously, we have successfully used an in-house developed code, Ambuild, to fully mimic synthetic procedures, including bond formation through a Sonogashira–Hagihara carbon–carbon coupling catalytic mechanism.[15] The acid catalysed triazine ring formation mechanism, shown in Fig. S2 (ESI†), proceeds *via* several protonated intermediates, **1**, **2**, and **3**. The first step is the protonation of the nitrogen of a cyano group on the monomer, and formation of the resultant carbocation to give intermediate **1**. To mimic this step, we assume that all cyano groups are protonated in this way, and therefore add a hydrogen to the nitrogen of the cyano groups. We also add a hydrogen to the carbon of the cyano group to enable bond formation to occur at this location and the carbon–nitrogen bond is changed from a triple to a double bond, with the respective double bond structure. These hydrogen centres act as cap atoms and the respective attached carbon and nitrogen atoms act as the end groups that allow the Ambuild code to determine bond vectors and bonding strategy. This results in the network building block used to grow the extended polymer.

We start by seeding one building block into the cell and use a growBlocks step to mimic the next step in the mechanism whereby a second block is bonded to the first block. The Ambuild code randomly identifies a free end group and attaches a second building block, following prescribed bonding rules: that a carbon end group can only bond to a nitrogen end group and *vice versa*. The orientation of the attached building block is determined by the cap atom vectors and we test for any close contacts with other atoms within the cell. When a successful bond is formed, the hydrogen cap atoms are removed. This forms the equivalent of intermediate **2**; the process is repeated to give intermediate **3**. To form a triazine ring from intermediate **3**, a zipBlocks test is undertaken; each end group is tested to see if it is possible to form a bond between it and neighbouring end groups, by determining the distance and angle between them and measuring against predetermined criteria. Upon a successful zipBlocks test, a bond is formed between the two end groups and the cap atoms removed.

The parameters used within Ambuild to describe the bonds, angles, and dihedrals are developed using a simplified test mechanism, calibrating against structures obtained from the PCFF-forcefield (see ESI,† Section S4 for full details). We are therefore confident that Ambuild can successfully replicate the triazine ring formation mechanism and the formation of intermediates.

The P1 extended structure is generated using the following protocol within the Ambuild code: (i) a single building block is seeded into a 50 Å × 50 Å × 50 Å cell, and the surrounding volume filled with equal parts chloroform and triflate counter ions; (ii) a loop is then entered, whereby the chloroform solvent and triflate is removed, a building block is added through a growBlocks step, the chloroform solvent and triflate are added back into the cell, and a structural optimisation is undertaken. A zipBlocks test is then undertaken, and if successful, the cell is optimised, (iii) this loop continues until no further building blocks can be grown within the cell. At this point we consider the network fully grown and remove any solvent or triflate anions to generate the representative final structure.

Network growth analysis

Fig. 2 and Fig. S11–S16 (ESI†) show snapshots of the P1 network growth. We can see approximations of the idealised CTF-1 *hca* 2-D topology start to form very early within the network growth. The P1 cluster grows as a relatively flat sheet but is distorted by the presence of solvent, triflate ions and by interaction with other parts of the network. These network interactions result in network interpenetration and distortions leading to the observed amorphous structure developing.

As the network grows, we can see the triazine rings (6-ring) form as expected but we also observe other ring features including four membered rings (4-ring, Fig. S17, ESI†) and eight membered rings (8-ring, Fig. S18, ESI†). We also observe structures that will lead to ring formation (pre-ring).

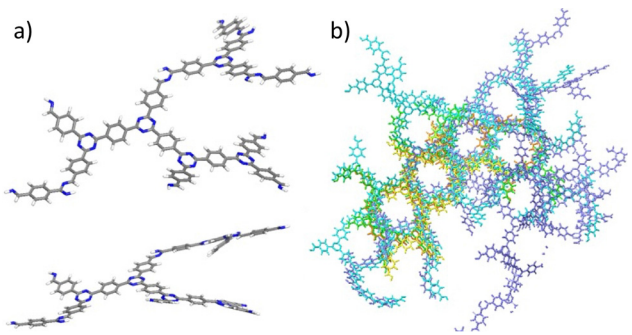

Fig. 2 (a) A snapshot of a CTF-1 fragment at step 15 of the polymer growth process. (b) An overlay of the CTF-1 polymer at different stages of the polymer growth process. Yellow – step 15, orange – step 27, green – step 36, blue – step-83, and purple – step 109.

The pre-4-ring can either go on to form a 4-ring feature or, with addition of a building block, form a pre-6-ring feature. Equally, the pre-6-ring can either form a 6-ring or *via* addition of a building block, form a pre-8-ring (Fig. S19, ESI†). The pre-8-ring can either form an 8-ring feature or *via* addition of a building block form a pre-10-ring, which we do not observe. These competing ring formation reactions also add to the amorphous nature of the resultant structure. Fig. S20 (ESI†) shows the number of ring features found within the structure as a function of the artificial synthesis step.

We can see that at all stages the triazine rings dominate in number, followed by pre-4-ring and pre-6-ring. This is as we would expect, as the reaction pathway is set up to follow this route and once a triazine ring is formed, it is unable to react further. Only a small number of 4-rings, pre-8-ring and 8-ring features are observed. Presumably, in a system where any C–N bond formation is reversible, such as using $ZnCl_2$ for CTF-1, then these network errors will be reversed and therefore not permanently form. Fig. S21 (ESI†) shows a macrocycle consisting of six phenyl rings and six triazine rings, a feature that would be observed in the idealised *hca* topological form, and Fig. S22 (ESI†) shows a spiral shaped feature in which the macrocycle did not 'complete' but continued to grow.

Network structure analysis and comparison to experiment

Fig. S23 (ESI†) shows the resulting P1 structure. Analysis of the solvent accessible surface area shows only very small pockets of non-connected porosity, resulting in a zero surface area in agreement with the experimentally determined BET surface area.[11] A fully amorphous system is generated (Fig. S24, ESI†), as reflected in the simulated PXRD pattern that shows no features evidencing crystallinity in agreement with the experimental results for P1.

Fig. S25 (ESI†) shows the experimental IR spectrum of CTF-1. Absorption peaks from unreacted cyano groups are observed at 2228 cm^{-1} and triazine rings at 1507 cm^{-1} and 1352 cm^{-1}. Fig. S26 (ESI†) shows the IR spectrum for P1. Similarly, a peak can be observed from unreacted cyano groups at $\sim$2200 cm^{-1} and triazine rings at $\sim$1500 cm^{-1} and $\sim$1300 cm^{-1}. However, additional peaks can also be observed at $\sim$1000 cm^{-1}, $\sim$1600 cm^{-1}, $\sim$2350 cm^{-1}, and a broad peak with features at $\sim$3200 cm^{-1}, $\sim$3400 cm^{-1} and $\sim$3600 cm^{-1}. Using literature data given in Table S2 (ESI†), some of these additional absorption peaks can be attributed to the presence of the protonated intermediates.

To test this theory, calculation of the IR spectra of fragments of the generated P1 structure were undertaken (see ESI,† Section S8 for details). Features included within the fragments include intermediates, ring structures, pre-ring structures, and triazine ring structures, shown in Fig. S27 (ESI†) with their respective calculated IR spectra. We can see that the wavenumber at which absorption occurs within the fragment spectra correlates well with the observed wavenumbers within the experimentally obtained spectra. It is noted that when the species is charged, such as for the fragment shown in Fig. S27(b) (ESI†), an intense peak at $\sim$3600 cm^{-1} is observed. When the charge is removed within the calculation, this peak is much reduced in intensity.

However, two identified features are present in the experimental spectra that are not accounted for in the set of CTF fragment simulated spectra. These are the set of peaks located at $\sim$2350 cm^{-1} and $\sim$3400 cm^{-1}. There are two rationalisations of this: (1) that there are structural features present that are not included in our models, or (2) the highly porous network has adsorbed guests from the atmosphere. We note that these peaks are located in the regions expected for carbon dioxide (peaks observed experimentally at $\sim$2350 cm^{-1} for matrix isolated molecules)[16] and water (a similarly broad peak observed experimentally at 3400 cm^{-1} for single water molecules absorbed within macromolecules)[17] which, combined with lack of any other experimental evidence for missing structural features, leads us to explore the option of the presence of these within the CTF micropore structure. CTF materials are known to be extremely carbon dioxide-philic with many CTF materials having exceptional carbon dioxide uptake with strong binding to the nitrogen-containing triazine rings. [18] The corresponding IR spectra for these CTF materials also show the same unexplained peaks.[18] Microporous materials in general are known to be highly absorbent to atmospheric water and carbon dioxide.[19]

The calculated spectrum for a single molecule of carbon dioxide is shown in Fig. S28 (ESI†). A peak is observed at 2350 cm^{-1} and a smaller peak at $\sim$500 cm^{-1}. Fig. S29(a) (ESI†) shows the spectrum for a single water molecule. We see a peak at $\sim$3600 cm^{-1} and a peak at $\sim$1700 cm^{-1}. Given the potential, due to the synthetic protocol, for protonated intermediates and the presence of water, it is also likely that hydronium ions will also be present. Fig. S29(b) (ESI†) shows the spectrum for a single hydronium ion. We see a peak at $\sim$3500 cm^{-1}, $\sim$1700 cm^{-1}, and at 1000 cm^{-1}. Using these calculated spectra, we can identify the potential origin of some key peaks, as shown in Fig. S30(a) and (b) (ESI†) shows the sum of the spectra for the neutral P1 fragments, carbon dioxide, water, and hydronium. It is known that the intensity of the peaks within the IR spectrum of water is proportional to the amount of water present as the absorption modes are intensified by the degree of the hydrogen bonding network formed.[17] As water within the P1 framework will be able to interact with neighbouring water and chemical features within the P1 structure, it is reasonable to scale the peaks of the single water molecule spectrum to generate its contribution to the overall spectra. Fig. 3 shows the summed simulated IR spectra with scaled water peaks in comparison to the experimental spectrum. An exact match to the experimental IR spectra is not possible as an exact composition of the P1 amorphous structure would be required, however we can now see that a good match to experiment is achieved. We can therefore conclude that P1 contains the chemical features contained within the fragment set, including neutral intermediates, rings, pre-rings, and triazine rings, and carbon dioxide, water, and hydronium ions within the pore structure.

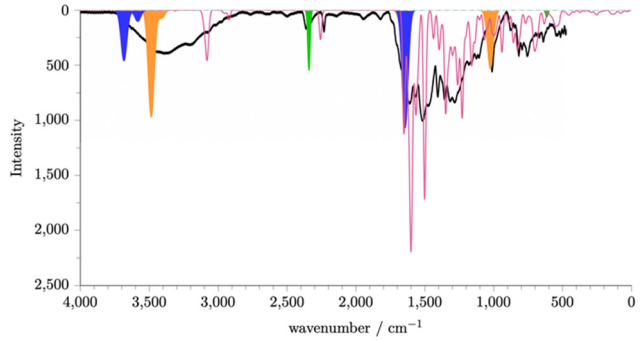

Fig. 3 Simulated and experimental (black line) spectra of P1. The simulated spectra of P1 (pink) is generated by summing together the simulated spectra generated for P1 fragments that we expect to be present within the P1 structure. See ESI,† Section S8 for details. The regions shaded blue, orange, and green can be rationalised as originating from absorbed water, hydronium ions, and carbon dioxide respectively.

Conclusions

We have shown that we are able to mimic the triazine ring formation mechanism and therefore generate realistic models incorporating structural features that would otherwise not be realised. Furthermore, it is only possible to replicate the experimental IR spectra by including structural diversity, network errors, and guests. This will aid in the design of triazine ring-containing materials and rationalisation of their properties.

Conflicts of interest

There are no conflicts to declare.

Notes and references

1 M. Eddaoudi, D. B. Moler, H. Li, B. Chen, T. M. Reineke, M. O'Keefe and O. M. Yaghi, Modular chemistry: secondary building units as a basis for the design of highly porous and robust metal-organic carboxylate frameworks, *Acc. Chem. Res.*, 2001, **34**, 319–330; S. Kitigawa, R. Kitaura and S. Noro, *Angew. Chem., Int. Ed.*, 2004, **43**, 2334–2375; S. S. Han and W. A. Goddard, Lithium-Doped Metal-Organic Frameworks for Reversible H2 Storage at Ambient Temperature, *J. Am. Chem. Soc.*, 2007, **129**(27), 8422–8423, DOI: 10.1021/ja072599+.

2 A. P. Côté, A. I. Benin, N. W. Ockwig, M. O'Keeffe, A. J. Matzger and O. M. Yaghi, Porous, crystalline, covalent organic frameworks, *Science*, 2005, **310**(5751), 1166–1170; J. R. Hunt, C. J. Doonan, J. D. LeVangie, A. P. Cote and O. M. Yaghi, Reticular synthesis of covalent organic borosilicate frameworks, *J. Am. Chem. Soc.*, 2008, 11872–11873; A. P. Cote, H. M. El-Kaderi, H. Furukawa, J. R. Hunt and O. M. Yaghi, *J. Am. Chem. Soc.*, 2007, **129**, 12914–12915; H. M. El-Kaderi, J. R. Hunt, J. L. Mendoza-Cortes, A. P. Cote, R. E. Taylor, M. O'Keefe and O. M. Yaghi, Designed synthesis of 3D covalent organic frameworks, *Science*, 2007, **316**, 268–272; S. Wan, J. Guo, J. Kim, H. Ihee and D. Jiang, A Belt-Shaped, Blue Luminescent, and Semiconducting Covalent Organic Framework, *Angew. Chem., Int. Ed.*, 2008, **47**, 1–5.

3 J. Germain, J. M. J. Fréchet and F. Svec, Nanoporous Polymers for Hydrogen Storage, *Small*, 2009, **5**(10), 1098–1111, DOI: 10.1002/smll.200801762; R. Dawson, A. I. Cooper and D. J. Adams, Nanoporous organic polymer networks, *Prog. Polym. Sci.*, 2012, **37**(4), 530–563, DOI: 10.1016/j.progpolymsci.2011.09.002; L. J. Barbour, Crystal porosity and the burden of proof, *Chem. Commun.*, 2006, 1163–1168, DOI: 10.1039/b515612m.; A. K. Cheetham, G. Ferey and T. Loieau, Open-Framework Inorganic Materials, *Angew. Chem., Int. Ed.*, 1999, **38**, 3268–3292; J. T. A. Jones, T. Hasell, X. Wu, J. Bacsa, K. E. Jelfs, M. Schmidtmann, S. Y. Chong, D. J. Adams, A. Trewin and F. Schiffman, *et al.*, Modular and predictable assembly of porous organic molecular crystals, *Nature*, 2011, **474**(7351), 367–371, DOI: 10.1038/nature10125. https://www.nature.com/nature/journal/v474/n7351/abs/10.1038-nature10125-unlocked.html#supplementary-information.

4 C. D. Wood, B. Tan, A. Trewin, H. Niu, D. Bradshaw, M. J. Rosseinsky, Y. Z. Khimyak, N. L. Campbell, R. Kirk and E. Stoeckel, *et al.*, Hydrogen Storage in Microporous Hypercrosslinked Organic Polymer Networks, *Chem. Mat.*, 2007, **19**, 2034–2048.

5 T. Ben, H. Ren, S. Ma, D. Cao, J. Lan, X. Jing, W. Wang, J. Xu, F. Deng and J. Simmons, *et al.*, Targeted Synthesis of a Porous Aromatic Framework with High Stability and Exceptionally High Surface Area, *Angew. Chem., Int. Ed.*, 2009, **48**(50), 9457–9460, DOI: 10.1002/anie.200904637; A. Trewin and A. I. Cooper, Porous Organic Polymers: Distinction from Disorder?, *Angew. Chem., Int. Ed.*, 2010, **49**(9), 1533–1535, DOI: 10.1002/anie.200906827.

6 J. Jiang, F. Su, A. Trewin, C. D. Wood, N. L. Campbell, H. Niu, C. Dickinson, A. Y. Ganin, M. J. Rosseinsky and Y. Z. Khimyak, *et al.*, *Angew. Chem., Int. Ed.*, 2007, **46**, 1–5; J. Weber and A. Thomas, Toward Stable Interfaces in Conjugated Polymers: Microporous Poly(p-phenylene) and Poly(phenyleneethynylene) Based on a Spirobifluorene Building Block, *J. Am. Chem. Soc.*, 2008, **130**(20), 6334–6335, DOI: 10.1021/ja801691x, (acccessed 2012/08/13).

7 N. B. McKeown and P. M. Budd, Polymers of intrinsic microporosity (PIMs): organic materials for membrane separations, heterogenous catalysis and hydrogen storage, *Chem. Soc. Rev.*, 2006, **35**, 675–683.

8 P. Kuhn, M. Antonietti and A. Thomas, *Angew. Chem., Int. Ed.*, 2008, **47**, 3450–3453.

9 P. Kuhn, A. Forget, D. Su, A. Thomas and M. Antonietti, From Microporous Regular Frameworks to Mesoporous Materials with Ultrahigh Surface Area: Dynamic Reorganization of Porous Polymer Networks, *J. Am. Chem. Soc.*, 2008, **130**(40), 13333–13337, DOI: 10.1021/ja803708s, (acccessed 2012/08/13)P. Kuhn, A. Thomas and M. Antonietti, *Macromolecules*, 2009, **42**, 319–326; M. J. Bojdys, J. Jeromenok, A. Thomas and M. Antonietti, Rational Extension of the Family of Layered, Covalent, Triazine-Based Frameworks with Regular Porosity, *Adv. Mater.*, 2010, **22**(19), 2202–2205, DOI: 10.1002/adma.200903436.

10 H. Wang, D. Jiang, D. Huang, G. Zeng, P. Xu, C. Lai, M. Chen, M. Cheng, C. Zhang and Z. Wang, Covalent triazine frameworks for carbon dioxide capture, *J. Mater. Chem. A*, 2019, **7**(40), 22848–22870, DOI: **10.1039/C9TA06847C**.

11 S. Ren, M. J. Bojdys, R. Dawson, A. Laybourn, Y. Z. Khimyak, D. J. Adams and A. I. Cooper, Porous, Fluorescent, Covalent Triazine-Based Frameworks Via Room-Temperature and Microwave-Assisted Synthesis, *Adv. Mater.*, 2012, **24**(17), 2357–2361, DOI: **10.1002/adma.201200751**.

12 A. Trewin, D. J. Willock and A. I. Cooper, Atomistic Simulation of Micropore Structure, Surface Area, and Gas Sorption Properties for Amorphous Microporous Polymer Networks, *J. Phys. Chem. C*, 2008, **112**(51), 20549–20559, DOI: **10.1021/jp806397f**; J.-X. Jiang, A. Trewin, F. Su, C. D. Wood, H. Niu, J. T. A. Jones, Y. Z. Khimyak and A. I. Cooper, Microporous Poly(tri(4-ethynylphenyl)amine) Networks: Synthesis, Properties, and Atomistic Simulation, *Macromolecules*, 2009, **42**(7), 2658–2666, DOI: **10.1021/ma802625d**.

13 C. Reece, D. J. Willock and A. Trewin, Modelling analysis of the structure and porosity of covalent triazine-based frameworks, *Phys. Chem. Chem. Phys.*, 2015, **17**(2), 817–823, DOI: **10.1039/C4CP04046E**.

14 H. Li, A. D. Chavez, H. Li, H. Li, W. R. Dichtel and J.-L. Bredas, Nucleation and Growth of Covalent Organic Frameworks from Solution: The Example of COF-5, *J. Am. Chem. Soc.*, 2017, **139**(45), 16310–16318, DOI: **10.1021/jacs.7b09169**.

15 J. M. H. Thomas, C. Mollart, L. Turner, P. Heasman, P. Fayon and A. Trewin, Artificial Synthesis of Conjugated Microporous Polymers via Sonogashira–Hagihara Coupling, *J. Phys. Chem. B*, 2020, **124**(33), 7318–7326, DOI: **10.1021/acs.jpcb.0c04850**.

16 D. F. Dinu, M. Podewitz, H. Grothe, T. Loerting and K. R. Liedl, Decomposing anharmonicity and mode-coupling from matrix effects in the IR spectra of matrix-isolated carbon dioxide and methane, *Phys. Chem. Chem. Phys.*, 2020, **22**(32), 17932–17947, DOI: **10.1039/D0CP02121K**.

17 Y. Maréchal, Observing the water molecule in macromolecules and aqueous media using infrared spectrometry, *J. Mol. Struct.*, 2003, **648**(1), 27–47, DOI: **10.1016/S0022-2860(02)00493-3**.

18 W. Yu, S. Gu, Y. Fu, S. Xiong, C. Pan, Y. Liu and G. Yu, Carbazole-decorated covalent triazine frameworks: Novel nonmetal catalysts for carbon dioxide fixation and oxygen reduction reaction, *J. Catal.*, 2018, **362**, 1–9, DOI: **10.1016/j.jcat.2018.03.021**; Q.-Q. Dang, C.-Y. Liu, X.-M. Wang and X.-M. Zhang, Novel Covalent Triazine Framework for High-Performance CO2 Capture and Alkyne Carboxylation Reaction, *ACS Appl. Mater. Interfaces*, 2018, **10**(33), 27972–27978; J. Li, P. Liu, H. Huang, Y. Li, Y. Tang, D. Mei and C. Zhong, Metal-Free 2D/2D Black Phosphorus and Covalent Triazine Framework Heterostructure for CO2 Photoreduction, *ACS Sustainable Chem. Eng.*, 2020, **8**(13), 5175–5183, DOI: **10.1021/acssuschemeng.9b07591**; Y.-M. Li, L. Yang, L. Sun, L. Ma, W.-Q. Deng and Z. Li, Chemical fixation of carbon dioxide catalyzed *via* covalent triazine frameworks as metal free heterogeneous catalysts without a cocatalyst, *J. Mater. Chem. A*, 2019, **7**(45), 26071–26076, DOI: **10.1039/C9TA07266G**; J. Roeser, K. Kailasam and A. Thomas, Covalent Triazine Frameworks as Heterogeneous Catalysts for the Synthesis of Cyclic and Linear Carbonates from Carbon Dioxide and Epoxides, *ChemSusChem*, 2012, **5**(9), 1793–1799, DOI: **10.1002/cssc.201200091**, (acccessed 2022/05/16).

19 R. Dawson, L. A. Stevens, T. C. Drage, C. E. Snape, M. W. Smith, D. J. Adams and A. I. Cooper, Impact of Water Coadsorption for Carbon Dioxide Capture in Microporous Polymer Sorbents, *J. Am. Chem. Soc.*, 2012, **134**(26), 10741–10744, DOI: **10.1021/ja301926h**.